The Journal of Immunology

RESEARCH ARTICLE | MARCH 05 2023

Lymphocytic Choriomeningitis Virus Clone 13 Infection Results in CD8 T Cell–Mediated Host Mortality in Diacylglycerol Kinase α–Deficient Mice

Matthew R. Kudek; ... et. al

J Immunol (2023) 210 (9): 1281–1291.
https://doi.org/10.4049/jimmunol.2101011

Lymphocytic Choriomeningitis Virus Clone 13 Infection Results in CD8 T Cell–Mediated Host Mortality in Diacylglycerol Kinase α–Deficient Mice

Matthew R. Kudek,*,†,‡ Gang Xin,†,1 Donia Alson,† Sandra Holzhauer,† Jian Shen,†,‡ Moujtaba Y. Kasmani,†,‡ Matthew Riese,†,§,2 and Weiguo Cui†,‡,3

Diacylglycerol is a potent element of intracellular secondary signaling cascades whose production is enhanced by cell-surface receptor agonism and function is regulated by enzymatic degradation by diacylglycerol kinases (DGKs). In T cells, stringent regulation of the activity of this second messenger maintains an appropriate balance between effector function and anergy. In this article, we demonstrate that DGKα is an indispensable regulator of TCR-mediated activation of CD8 T cells in lymphocytic choriomeningitis virus Clone 13 viral infection. In the absence of DGKα, Clone 13 infection in a murine model results in a pathologic, proinflammatory state and a multicellular immunopathologic host death that is predominantly driven by CD8 effector T cells. ***The Journal of Immunology*****, 2023, 210: 1281–1291.**

Diacylglycerol (DAG) is a ubiquitous intracellular signaling molecule that accumulates at the cell membrane after receipt of an extracellular stimulus, typically by a G protein–coupled receptor (1) or by a TCR (2) or BCR (3) in lymphocytes to promote secondary signaling mechanisms. After cell-surface receptor agonism, phospholipase C is activated, hydrolyzing phosphatidylinositol 4,5-bisphosphate into DAG and inositol triphosphate. The accumulation of intracellular DAG recruits and activates Ras-GTPases and protein kinase C, triggering secondary signaling pathways associated with cell proliferation and survival (4).

Conversely, cell-surface receptor agonism also recruits members of the DAG neutralizing family of enzymes, DAG kinases (DGKs), to the immunologic synapse (5). Mechanistically, DGKs cleave DAG into phosphatidic acid to deactivate DAG-mediated secondary signaling pathways. Ten known isoforms of DGK have been identified in mammals (6), and they are classified into five subgroups based on their regulatory motifs. Isoforms are incompletely redundant (6) in their specific functional control, and most DGK isoforms are expressed in multiple tissues. Multiple isoforms can also be present within the same tissue or cell type (2). Mutations and polymorphisms of DGK isoforms are implicated in diseases, including hypospadias (κ) (7), psychiatric disorders (η) (8), diabetes mellitus (ε, ζ), atypical hemolytic uremic syndrome (ε), and cancer progression (α) (9).

In lymphocytes, tight regulation of DAG activity and metabolism manages a balance in activated T cells between effector function and anergy. Olenchock et al. (10) showed that combined TCR stimulation with CD28 costimulation significantly increases production of DAG and leads to downregulation of two DGK isoforms (α and ζ) intrinsic to T cells. In contrast, isolated TCR stimulation leads to lowered production of DAG and increased DGKα (10).

In models of forced overexpression of DGKα, there is significantly impaired T cell activation. This occurs as a result of impaired transcription of activator protein-1 (AP-1) family transcription factors (11), which normally heterodimerize with NFAT to upregulate the transcription of key molecules involved in T cell activation, including IL-2, IL-3, IL-4, and GM-CSF (12). Consequently, the lack of AP-1 members results in unpartnered NFAT, inadequate transcription, and an anergic T cell state (13).

Because the absence of DGKα in an acute infection model has been shown to enhance effector T cell response and promote viral clearance when compared with wild-type (WT) controls (14), we hypothesized that a similar effect would be observed in a chronic

*Division of Pediatric Hematology, Oncology, and BMT, Department of Pediatrics, Medical College of Wisconsin, Milwaukee, WI; †Versiti Blood Research Institute, Milwaukee, WI; ‡Department of Microbiology and Immunology, Medical College of Wisconsin, Milwaukee, WI; and §Division of Oncology, Department of Medicine, Medical College of Wisconsin, Milwaukee, WI

[1]Current address: Department of Microbial Infection and Immunity, Ohio State University, Columbus, OH.

[2]Deceased.

[3]Current address: Department of Pathology, Northwestern University, Feinberg School of Medicine, Chicago, IL.

ORCIDs: 0000-0002-4140-6707 (M.R.K.); 0000-0001-5033-3696 (D.A.); 0000-0001-8398-2318 (J.S.); 0000-0002-5753-5335 (M.Y.K.); 0000-0003-1562-9218 (W.C.).

Received for publication October 21, 2021. Accepted for publication February 21, 2023.

This work was supported by the St. Baldrick's Foundation Fellowship (812679 to M.R.K.). M.Y.K. is a member of the Medical Scientist Training Program at the Medical College of Wisconsin, which is partially supported by a training grant from National Institute of General Medical Sciences, National Institutes of Health (T32-GM080202). W.C. was supported by National Institute of Allergy and Infectious Diseases, National Institutes of Health Grants AI125741 and AI148403, by an American Cancer Society Research Scholar Grant, and by an Advancing a Healthier Wisconsin Endowment Grant.

Conceptualization, M.R.K., G.X., S.H., M.R., and W.C.; investigation, M.R.K., G.X., D.A., S.H., J.S., and M.Y.K.; data analysis, M.R.K. and M.Y.K.; manuscript preparation, M.R.K.; writing—review and editing, M.R.K., G.X., S.H., M.Y.K., and W.C.; supervision, W.C.; all authors have read and agreed to the published version of the manuscript.

The Bulk RNA sequencing data presented in this article have been submitted to the Gene Expression Omnibus database (https://www.ncbi.nlm.nih.gov/geo/query/acc.cgi?acc=GSE186256) under accession number GSE186256.

Address correspondence and reprint requests to Dr. Matthew R. Kudek or Dr. Weiguo Cui, Department of Pediatrics, Division of Pediatric Oncology, Medical College of Wisconsin, 8701 West Watertown Plank Road, MFRC 3018, Milwaukee, WI 53226 (M.R.K.) or Department of Pathology, Northwestern University, Feinberg School of Medicine, 303 E Chicago Avenue, Chicago IL 60611 (W.C.). E-mail addresses: mkudek@mcw.edu (M.R.K.) or weiguo.cui@northwestern.edu (W.C.)

The online version of this article contains supplemental material.

Abbreviations used in this article: AP-1, activator protein-1; DAG, diacylglycerol; DGK, diacylglycerol kinase; GCB, germinal center B cell; GSEA, gene set enrichment analysis; IFN-I, type I IFN; LAG-3, lymphocyte-activation gene 3; LCMV, lymphocytic choriomeningitis virus; MFI, mean fluorescent intensity; mTOR, mammalian target of rapamycin; p.i., postinfection; PD-1, programmed cell death protein 1; PTP, protein tyrosine phosphatase; RNA-seq, RNA sequencing; Tfh, T follicular helper; Treg, regulatory T cell; WT, wild-type.

infection model. A prototypic model of chronic infection is the lymphocytic choriomeningitis virus (LCMV) Clone 13 strain. LCMV Clone 13 is an advantageous model because the virus is noncytopathic, ensuring that phenotypic observations within the host are a direct result of the host immune response and not viral cytotoxicity. Clone 13 infection in an immunocompetent host leads to a phenotype of persistent viral infection and T cell exhaustion. As a result of exhaustion, CD8 T cells develop dysfunction in their ability to proliferate and in their ability to produce IL-2, TNF-α, and IFN-γ. Further, exhausted T cells demonstrate high levels of inhibitory receptors, including programmed cell death protein 1 (PD-1) and lymphocyte-activation gene 3 (LAG-3). PD-1 signaling is also shown to limit signaling through the mammalian target of rapamycin (mTOR) pathways and inhibit glycolysis (15).

We report our findings of unexpected mortality from an overwhelming immune response after LCMV Clone 13 infection in mice with germline DGKα deficiency. We further identified the same outcome occurs when DGKα deficiency is isolated to CD8 T cells, and that DGKα deficiency in CD8 T cells is necessary for the observed mortality and contributes to an enhanced effector phenotype in virus-specific CD8 T cells. In this study, we demonstrate that DGKα limits pathologic immune responses to Clone 13 infection, and we characterize the effect of DGKα in innate and adaptive immune responses in this model.

Materials and Methods

Mice

Mice deficient in DGKα were described previously (10). C57BL/6 mice were purchased from the National Cancer Institute. P14 mice, with transgenic expression of a TCR cognate to the LCMV epitope gp33 were maintained in-house. P14 DGKα$^{-/-}$ mice were generated through crossing DGKα$^{-/-}$ with P14 mice in-house. All experiments were performed in mice 6–12 wk old. Animal housing and experimentation were done in accordance with the guidelines of the Institutional Animal Care and Use Committee at the Medical College of Wisconsin.

Generation of CD8 T cell–restricted DGKα$^{-/-}$ mice by bone marrow chimera

Mice were generated with DGKα deficiency restricted to CD8 T cells by bone marrow chimera. Irradiation was delivered to CD45.1$^{+/+}$ recipient mice, followed by retroorbital injection of 2×10^6 total nucleated cells, comprised of single-cell suspension of bone marrow cells derived from a CD8$^{-/-}$ mouse (70%) and a CD45.2$^{+/+}$ DGKα-deficient mouse (30%). Control mice were also generated by the same protocol but were C57BL/6, CD45.2$^{+/+}$ hosts and received bone marrow cells derived from a CD8$^{-/-}$ mouse (70%) and a C57BL/6 CD45.1$^{+/+}$ mouse (30%). Recipient mice were CD8 T cell depleted by treatment with *InVivo*Plus anti-mouse CD8a mAb (clone YTS 169.4; BioXCell), and CD8 T cell reconstitution was confirmed by flow cytometry.

Statistics

Statistical analysis was performed using GraphPad Prism software (La Jolla, CA). Survival curve comparisons were performed using the log rank (Mantel–Cox) test. Weight curve comparisons were performed by mixed effect analysis with the Geisser–Greenhouse correction for variability and Bonferroni correction for multiple comparisons with an α value of 0.05. Comparisons between frequency of cell subsets among experimental phenotypes were performed using an unpaired Welch's *t* test for cohorts with samples ≥5, or an unpaired Mann–Whitney *U* test for cohorts with sizes <5. Serum analytes were compared using an unpaired Mann–Whitney *U* test, using the Bonferroni correction for multiple comparisons, with an α value of 0.05. Paired *t* test was used for competitive assay/cotransfer experiments. A *p* value <0.05 was considered to indicate statistical significance (*$p < 0.05$, **$p < 0.01$, ***$p < 0.001$, and ****$p < 0.0001$).

LCMV infection

Infection with LCMV Clone 13 was achieved by inoculation of at least 2.5×10^6 PFUs or 5×10^6 focus-forming units, injected in 500 μl by retroorbital i.v. injection.

Peripheral blood sampling

Peripheral blood sampling was obtained by submandibular facial bleed. After vein puncture, three to four drops of fresh blood were collected directly into a heparinized capillary tube. Blood was then emptied from the capillary tube into an empty 1.5-ml mini-Eppendorf tube. Immediately, 20 μl of fresh blood was transferred into 120 μl of CellPak (Sysmex) diluent augmented with 5 mM EDTA (Fisher Scientific) and 0.5 μg/ml PGE_1 (Sigma-Aldrich). Samples were stored on ice until analysis on Sysmex XN-1000 Hematology Analyzer (Sysmex).

Serum viral titers

Immediately before mouse euthanasia, 100 μl of peripheral blood was obtained by submandibular facial bleed. Blood was stored at room temperature for ~2 h until coagulated and then was centrifuged at $1500 \times g$ for 15 min at 4°C. After centrifugation, serum comprised the supernatant, which was collected and stored at −20°C or −80°C until use in a focus-forming assay.

Serum cytokine analysis

Mouse Cytokine Array/Chemokine Array 31-Plex (MD31) was performed by Eve Technologies (Calgary, AB, Canada). Serum was isolated as described earlier. Reported results included serum levels of eotaxin, G-CSF, GM-CSF, IFN-γ, IL-1α, IL-1β, IL-2, IL-3, IL-4, IL-5, IL-6, IL-7, IL-9, IL-10, IL-12 (p40), IL-12 (p70), IL-13, IL-15, IL-17A, IP-10, keratinocyte chemoattractant, LIF, LPS-induced CXC chemokine, MCP-1, M-CSF, monokine induced by IFN-γ, MIP-1α, MIP-1b, MIP-2, RANTES, TNF-α, and vascular endothelial growth factor. For replicates with results that were either more than or less than the detectable limit of the assay, these samples were designated with the highest or lowest value obtained for that analyte, respectively, as recommended by the reference laboratory.

Focus-forming assay

Mouse serum containing LCMV Clone 13 was incubated in three serial dilutions with 3×10^4 Vero cells at 37°C, 5% CO_2 for 20 h, then fixed with 5% paraformaldehyde. After blocking (50 mM Tris, 0.14 M NaCl, 1% BSA) for 60 min at room temperature, wells were washed with PBS, and rat anti-LCMV nucleoprotein mAb (clone VL-4; BioXCell) was added and incubated overnight at 4°C. After unbound Ab was washed from wells with PBS, secondary staining was performed using goat anti-rat IgG2a-FITC (clone A110-109F; Bethyl) and imaged using the Incucyte Live Cell Analysis System (Essen Bioscience). Fluorescent foci were counted manually (DotDotGoose open-source software; American Museum of Natural History Center for Biodiversity and Conservation), and titers were calculated as focus-forming units per milliliter.

Cellular phenotyping

Cell types were classified as follows: CD4 regulatory T cell (Treg): CD4$^+$, CD25$^{+/-}$, and FOXP3$^+$; CD4 Th1: CD4$^+$, CD44$^+$, and CXCR6$^+$; CD4 T follicular helper (Tfh): CD4$^+$, CD44$^+$, and CXCR5$^+$; macrophage: CD11b$^+$ and F4/80$^+$; monocyte: CD11b$^+$, F4/80$^-$, Ly6C^{high}, and Ly6G$^-$; granulocyte: CD11b$^+$, F4/80$^-$, Ly6C^{int}, and Ly6G$^+$; virus-specific CD8 T cell: CD8$^+$, CD44$^+$, and gp33$^+$; and germinal center B cell (GCB): B220$^+$, Fas$^+$ and GL7$^+$. Single-cell suspensions of splenocytes were stained as follows. For myeloid subsets, surface stains included: Ly6C-FITC (clone HK1.4), F4/80-PE/Cy7 (BM8), Ly6G-allophycocyanin/Fire750 (1A8), and CD11b-Pacific Blue (M1-70). For Treg cells, surface stains included CD4-PE (GK1.5) and CD25-allophycocyanin (PC61), and transcription factor staining was performed using FOXP3-eFluor450 (FJK-16s; Invitrogen). CD4$^+$ T cells were stained using CXCR6-PE/Cy7 (SA051D1), CXCR5-allophycocyanin (L138D7), PD1-allophycocyanin/Cy7 (29F.1A12), CD44-Pacific Blue (IM7), and CD4-BV510 (RM4-5). CD8 T cells were stained using CD8-FITC (53-6.7), gp33 tetramer-PE (NIH Tetramer Core Facility), PD1-PE/Cy7 (RMP1-30), LAG3-PerCP/Cy5.5 (C9B7W), CD44-allophycocyanin/Cy7 (IM7), B220-PE-Cy7 (RA3-6B2), Fas-PE (SA367H8), and GL7-FITC (GL7). Intracellular stains include granzyme B-PE/CF594 (QA16A02) and IFN-γ-FITC (XMG1.2) All Abs were purchased from BioLegend, unless otherwise noted. Data were collected using a FACSLSRII or a FACSCelesta flow cytometer (BD Biosciences) with FACSDiva acquisition software. Data analysis was performed using FlowJo software (Tree Star).

RNA sequencing

Peripheral blood was obtained from a CD45.1$^{+/+}$ congenic marked P14 TCR transgenic C57BL/6 mouse and a CD45.1$^{+/+}$ DGKα$^{-/-}$ P14 mouse by submandibular bleed. Buffy coat was isolated by density centrifugation (Histopaque-1077; Sigma-Aldrich), and CD8 T cells were enriched by immunomagnetic negative selection (EasySep Mouse CD8$^+$ T cell Isolation Kit; STEMCELL Technologies). On microscopy, 100% viability was grossly

observed postenrichment by trypan blue staining. CD8 T cell suspension was diluted to 6×10^3 cells/ml. C57BL/6 recipient mice were inoculated with 2.5×10^6 PFUs of LCMV Clone 13 in 500 μl DMEM and either 3×10^3 CD45.1$^{+/+}$ DGKα$^{-/-}$ P14 CD8 T cells or 3×10^3 CD45.1$^{+/+}$ P14 CD8 T cells. Four biological replicates were included in each experimental condition. On day 8 postinfection (p.i.), mice were sacrificed, spleens were harvested, and single-cell suspension of splenocytes was obtained by mashing tissue against a cell strainer followed by erythrocyte lysis (ACK Lysis Buffer; Lonza). CD8 T cells were enriched by cell sorting (FACSMelody; BD) by gating on CD8$^+$ Ly5.1$^+$7AAD$^-$ cells. The recovered cell counts of DGKα$^{-/-}$ P14 cells and WT P14 T cells were not significantly different. After sorting, cDNA was prepared using established protocols (16). One nanogram of amplified cDNA from each mouse was used to generate a DNA library using the Nextera XT DNA Library Preparation Kit (Illumina). Four replicates from each group were subsequently sequenced. Uniquely barcoded libraries were pooled and sequenced with a NextSeq 500 sequencer using a NextSeq 500/550 high-output V2 75 cycle kit (Illumina) with the following configuration: read 1, 38 cycles; read 2, 38 cycles; index read 1, 8 cycles; and index read 2, 8 cycles. Bulk RNA sequencing (RNA-seq) data were aligned to the *Mus musculus* mm10 genome, and gene expression was quantified using Salmon (17). A single biological replicate of the WT cohort was excluded from subsequent analyses based on quality control. RNA-seq libraries were then normalized, and genes were tested for differential expression between DGKα-deficient and WT CD8 T cells with DESeq2 v1.24.0 (18). DESeq2 Wald tests were used to determine whether fold changes were significantly different from zero. For visualization, data were transformed using the regularized logarithmic transformation (18). Preranked gene set enrichment analyses (GSEAs) were conducted using shrunken fold changes and clusterProfiler v3.12.0 (19). Kyoto Encyclopedia of Genes and Genomes (20), Reactome (21), and Gene Ontology (22) databases were used for GSEA. The Benjamini–Hochberg method was used to adjust p values for false discovery in both differential expression analyses and GSEAs.

Competitive adoptive transfer

Peripheral blood was collected by facial bleed from age-matched female P14 and P14 DGKα$^{-/-}$ mice, and buffy coat was isolated by density centrifugation (Lymphoprep; STEMCELL Technologies). Each recipient mouse (C57BL/6) received congenic marked 2×10^3 P14 CD8 T cells and 2×10^3 P14 DGKα$^{-/-}$ CD8 T cells, along with concomitant LCMV Clone 13 infection. On day 8 p.i., spleens were harvested and processed into a single-cell suspension. One million cells per mouse were taken for staining and analysis by flow cytometry. An in vitro stimulation assay was also performed by taking 1×10^6 splenocytes per mouse, which were cultured with 0.1 μg of gp33 monomer, brefeldin A (BioLegend) and PE-CD107a (1D4B; BioLegend) for 6 h at 37°C, 5% CO2, and then were subsequently processed for flow cytometry. Cellular fixation and intracellular staining were performed using the Cytofast Fix/Perm Buffer Set (BioLegend).

CD8 T cell depletion

DGKα$^{-/-}$ mice were pretreated (day −1) with either 400 μg of CD8-depleting Ab (clone 2.43; InVivoMab) in 500 μl PBS or PBS alone by i.p.

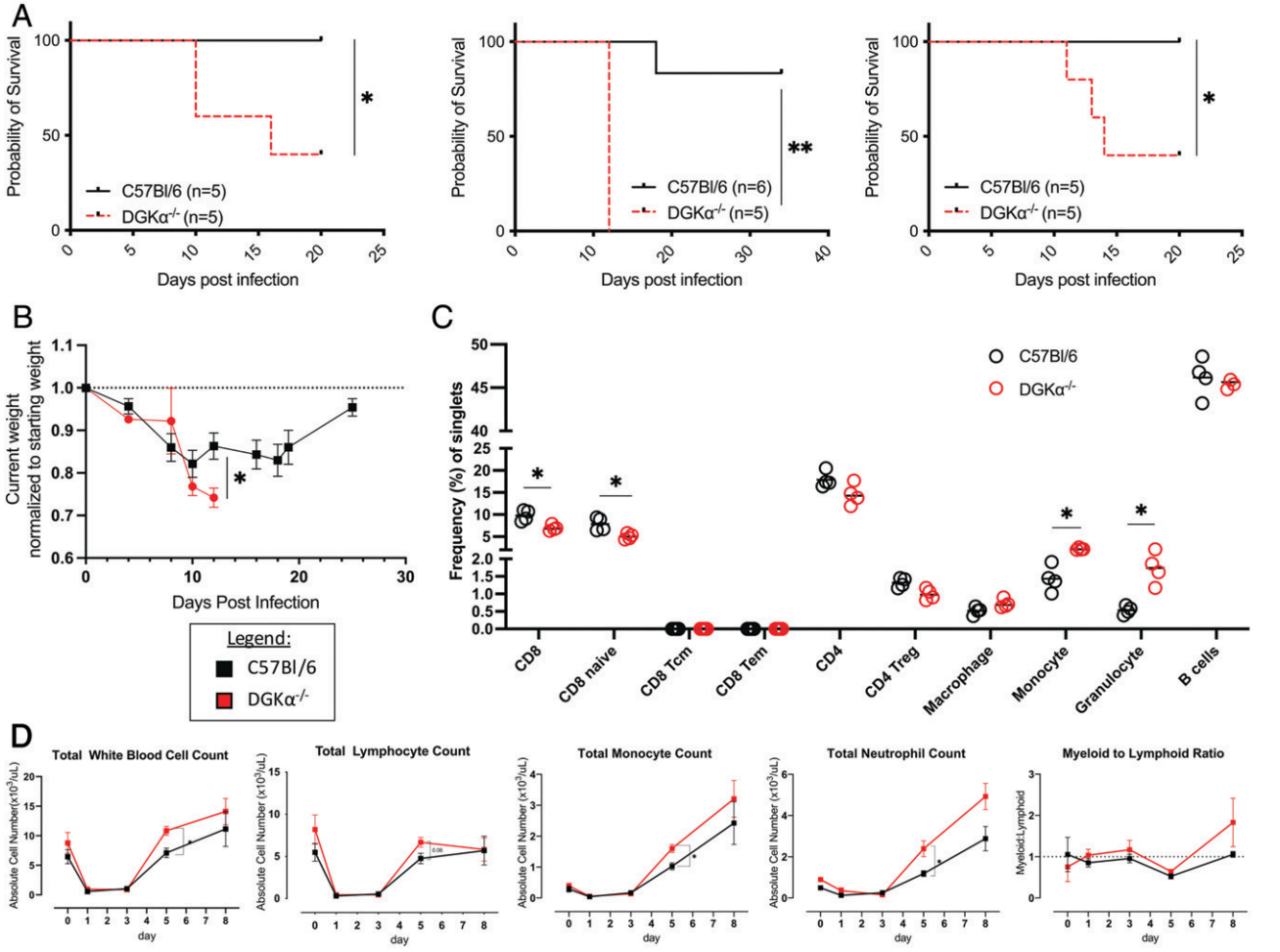

FIGURE 1. Characteristics of treatment cohorts p.i. with LCMV Clone 13. (**A**) Survival outcomes stratified by infection type in WT (C57BL/6) or DGKα$^{-/-}$ host. Three replicate experiments with their subsequent survival outcomes are shown. (**B**) Average change in host weight of treatment cohorts as a proportion of starting weight ($n = 5$ per cohort, single experiment). (**C**) Baseline composition of splenocytes from C57BL/6 and DGKα$^{-/-}$ mice before infection with LCMV Clone 13. (**D**) Total peripheral blood leukocyte, lymphocyte, monocyte, and neutrophil counts, and myeloid/lymphoid ratio before (day 0) and after LCMV Clone 13 infection. Peripheral blood counts are representative of $n = 6$ mice per cohort from two experiments. Error bars, when present, represent SEM. *$p < 0.05$, **$p < 0.01$.

injection. Mice were subsequently infected with LCMV Clone 13 by i.v. injection on day 0. Mice were weighed thrice weekly, and analysis for CD8 T cell depletion was performed by flow cytometric analysis of peripheral blood on day 7. For the duration of the study, mice were redosed weekly with either 250 μg of CD8-depleting Ab in PBS or an equivalent volume of PBS.

Data and code availability

Bulk RNA sequencing (RNA-seq) data from this article are available in the GEO database under accession code GSE186256 (https://www.ncbi.nlm.nih.gov/geo/query/acc.cgi?acc=GSE186256). All other raw data and scripts are available from the corresponding author on request.

Results

LCMV Clone 13 infection leads to mortality and severe weight loss in DGKα$^{-/-}$ hosts

We first used a systemic loss-of-function model to determine the role of DGKα in Clone 13 infection. p.i. with LCMV Clone 13, DGKα$^{-/-}$ mice suffered mortality (Fig. 1A), with a median survival time of 12 d. When combining all experimental replicates, 27% of the DGKα$^{-/-}$ cohort survived to the completion of the study, compared with 94% of the WT cohort ($p < 0.0001$). Mice deficient in DGKα also suffered more severe weight loss after Clone 13 infection (Fig. 1B). This cohort demonstrated persistent progression of weight loss during the observed period, with a mean of 26% loss of baseline weight on day 12 p.i. versus 14% weight loss in WT mice on day 12 p.i. ($p = 0.014$).

Clone 13 infection leads to enhanced peripheral immune cell expansion in DGKα$^{-/-}$ hosts

In the setting of this profound morbidity and mortality with LCMV Clone 13 infection, we hypothesized that the cause of death was an overwhelming immune response. To test this, we compared immune cell subsets for observable differences between the two groups at baseline. An immunophenotype of splenocytes at baseline (preinfection) revealed small, but significant decreases in total CD8 T cells and naive CD8 T cells in DGKα$^{-/-}$ mice and increases in monocyte and granulocyte subsets of myeloid cells (Fig. 1C). Peripheral blood was sampled at preinfection (day 0) and days 1, 3, 5, and 8 after LCMV Clone 13 infection (Fig. 1D). On day 5 p.i., the DGKα$^{-/-}$ mice had a significantly higher average total white blood count, with significant increases in absolute monocyte and neutrophil (granulocyte) counts. There was also a nonsignificant trend toward the same in lymphocytes. Similar trends persisted through day 8 p.i., although they were not statistically significant. p.i. myeloid/lymphoid cell ratios trended higher in the DGKα$^{-/-}$ group p.i. compared with control (Fig. 1D). Because most changes in peripheral white cell counts of DGKα$^{-/-}$ persisted through the day 8 time point, shortly before mice first began to die around day 10 (Fig. 1A), this suggested that a systemic proinflammatory state persisted until mortality.

Circulating analytes were subsequently compared in serum samples obtained from DGKα-deficient mice and WT mice in an uninfected state (day 0) and day 8 p.i. with LCMV Clone 13 (Fig. 2). There were no statistically significant differences between groups in assayed analytes at either time point when correcting for multiple hypotheses. An increase in IL-17 serum levels was observed in day 8 p.i. DGKα$^{-/-}$ mice as compared with day 8 p.i. WT mice (2.9 versus 0.43 pg/ml, respectively) with a trend toward significance ($p = 0.15$). IL-17 is produced by activated T cells and may mediate inflammation through recruitment of myeloid cells (23).

DGKα$^{-/-}$ increases myeloid-derived cells in early Clone 13 infection and has a blunted Tfh response

With the observed increases in WBC types in the peripheral blood, we next analyzed the role of DGKα in splenic immune cell subsets after Clone 13 infection. For this we performed flow cytometry on splenocytes harvested on day 8 p.i. We elected to use day 8 p.i. as our time point to harvest splenocytes because host mortality began occurring as early as day 10 p.i. in DGKα$^{-/-}$ hosts (Fig. 1A). Significant increases in frequency of myeloid cells were observed in DGKα$^{-/-}$ mice (Fig. 3A, 3B). There was no difference observed in the frequency of splenic macrophages, monocytes, or granulocytes, suggesting that the increase in total myeloid cells was not due to a skewed response from a particular myeloid subset (Fig. 3C–G). Others have previously reported that Clone 13 infection leads to enhanced expansion of splenic monocytic and neutrophilic cells by day 7 p.i., when

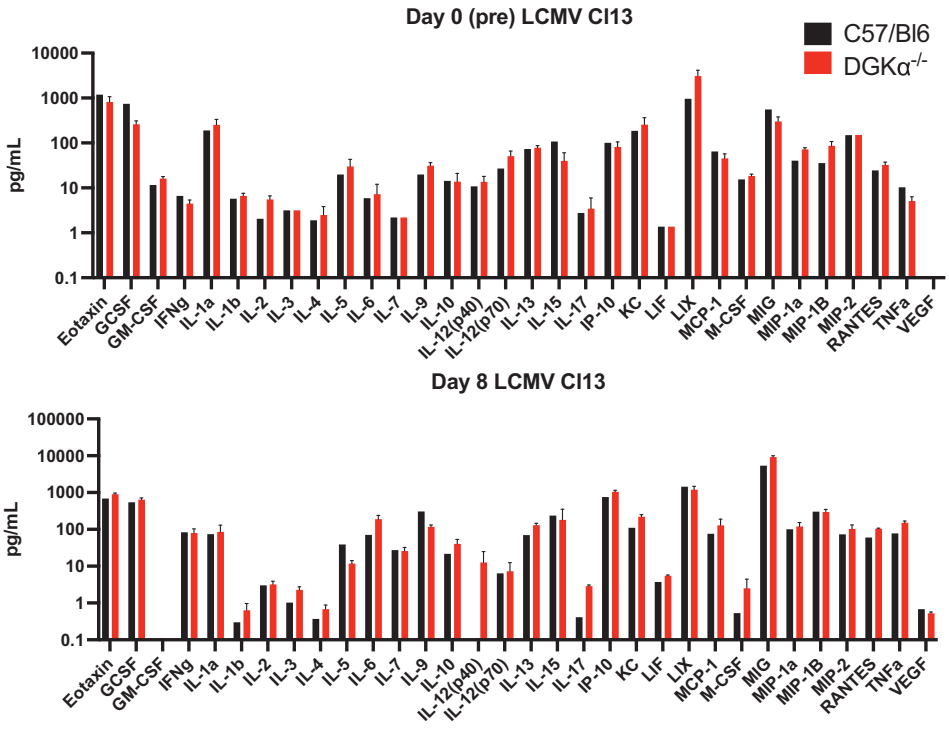

FIGURE 2. Serum measurements of selected cytokines at baseline, before infection (top; $n = 4$ per group, all collected at a single time point), and at day 8 after LCMV Clone 13 infection (bottom; $n = 3$ per group, all collected after a single infection). Vascular endothelial growth factor (day 0) and GM-CSF (day 8) serum levels were less than the assayable range in all samples. VEGF, vascular endothelial growth factor.

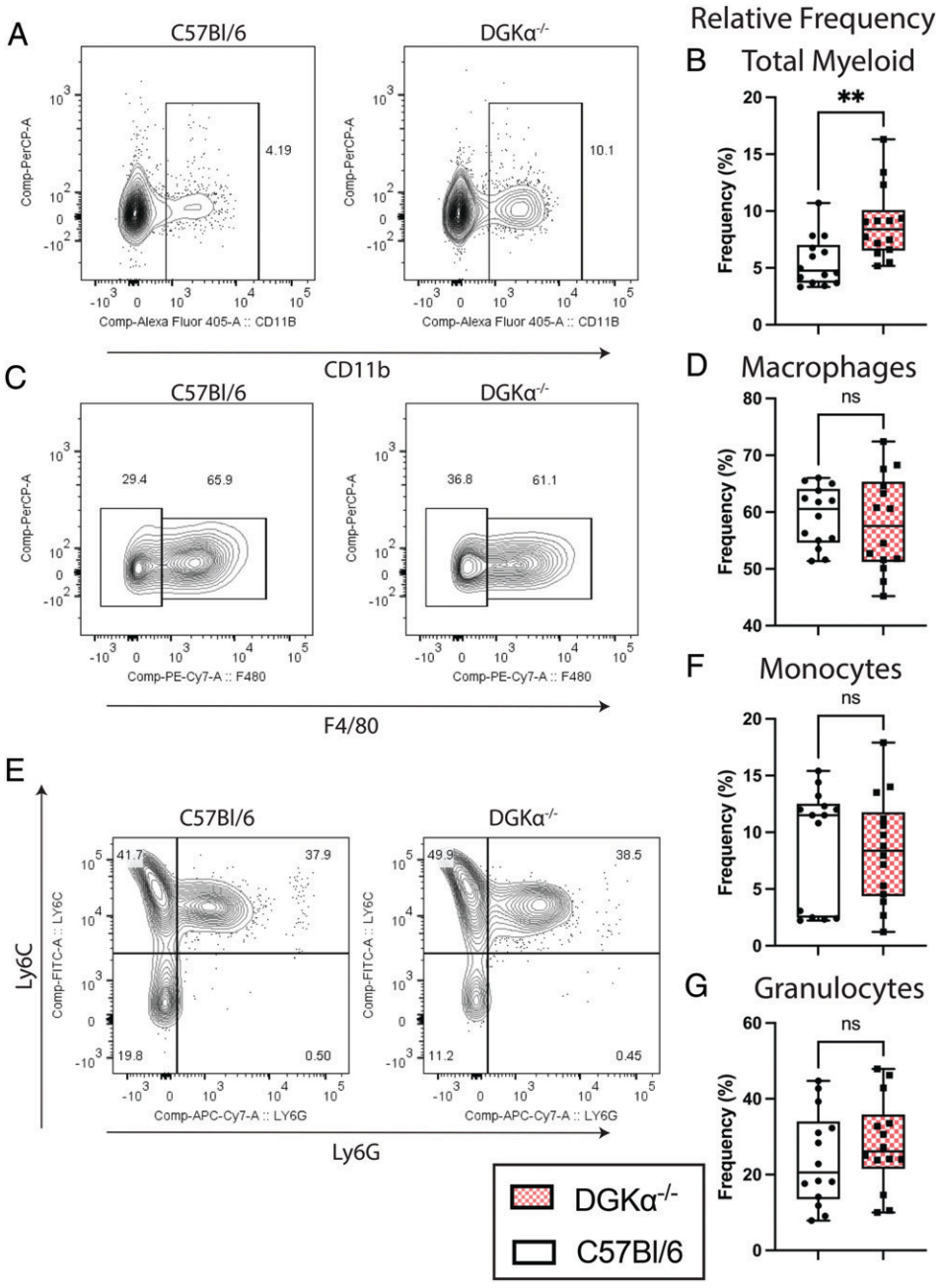

FIGURE 3. Relative frequencies of myeloid cell subsets among splenocytes on day 8 after LCMV Clone 13 infection. Representative flow plot and box and whisker plot for total splenic myelocytes (**A** and **B**), macrophages (**C** and **D**), monocytes, and granulocytes (**E**–**G**). Box plots demonstrate interquartile range and median; whisker error bars span from minimum to maximum values. Graphed relative frequency percentages are based on a ratio of the cell type listed to the following denominator listed in parentheses: total myelocyte (singlet splenocytes); and macrophages, monocytes, and granulocytes ($CD11b^+$ splenocytes). Data shown in the box and whisker plots are from 14 mice in total, aggregated from three independent infections. $^{**}p < 0.01$.

compared with Armstrong infection (24). Increased hematopoiesis with myeloid differentiation is associated with elevated levels of cytokines, including TNF-α and IL-6 (25). We observed nonsignificant trends toward an increase in these two cytokines in DGKα-deficient mouse serum at day 8 p.i. compared with WT. Others have shown that splenic myeloid cells remain fully capable of stimulating T cell production in early (day 7 p.i.) Clone 13 infection (24), which may contribute to our observed proinflammatory phenotype in our assessments at day 8 p.i.

We also compared the prevalence of Tregs between the WT and DGKα-deficient states. As expected in an early Clone 13 infection, there was no significant difference in the frequency of Tregs between experimental states (Fig. 4A, 4B). We further observed a decrease in the relative frequency of Tfh cells in $DGK\alpha^{-/-}$ mice (Fig. 4C, 4D), which is in line with previous research showing that virus-induced MDSCs can suppress Tfh responses (26). Further, there was no difference in effector Th1 cells between genotypes (Fig. 4E), which suggests that DGKα is not essential for limiting the Th1 cell activation in early chronic infection. Paradoxically, there was a significant increase in the frequency of GCBs within the spleen (Fig. 4F, 4G). Previous studies have supported the role of DAG signaling in early plasma cell formation and enhanced Ab production when DGKζ is absent (3). Our data suggest that DGKα may also be critical to attenuating GCB proliferation mediated by DAG signaling after Clone 13 infection, and this may be independent of Tfh interaction.

DGKα deficiency leads to enhanced CD8 T cell activation to early chronic viral infection and directly contributes to host mortality

Despite knowledge that DGKα functions to limit TCR signaling (27), we did not identify a role for DGKα in limiting Th1 T cell expansion as a cause of a mortal immune response in early Clone 13 infection. We therefore hypothesized that DGKα was crucial to balancing the CD8 T cell response in a chronic viral infection to prevent a pathologic immune response. To test this, we examined

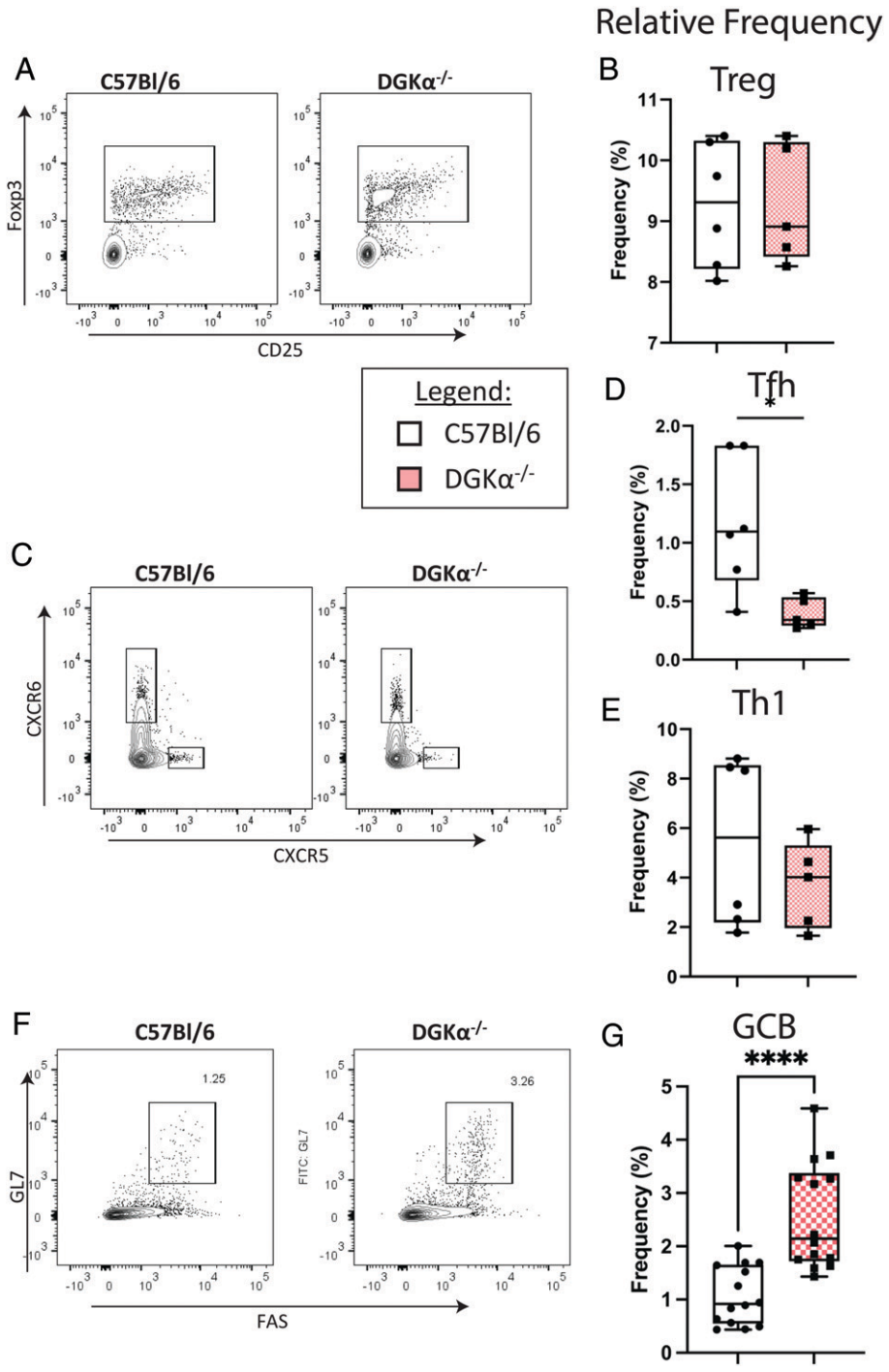

FIGURE 4. Relative frequencies of CD4 lymphoid and germinal center (GCB) cell subsets among splenocytes on day 8 after LCMV Clone 13 infection. Representative flow plots and box and whisker plots for Tregs (**A** and **B**), Tfh and Th1 (**C**–**E**), and GCB (**F** and **G**). Box plots demonstrate interquartile range and median; whisker error bars are from minimum to maximum values. Relative frequency percentages are based on a ratio of the cell type listed to the following denominator listed in parentheses: Treg, Tfh, and Th1 (CD4 splenocytes); and GCB (B220 splenocytes). Data presented in (A)–(E) represent a single experiment and infection, whereas data in (F) and (G) are aggregated from three experiments with independent infections. $*p < 0.05$, $****p < 0.0001$.

splenic LCMV-specific CD8 T cells by flow cytometry. In contrast with our findings in cytotoxic CD4 T cells on day 8 p.i., we identified a significant increase in the relative frequency of activated, virus-specific CD8 T cells in the DGKα$^{-/-}$ host (Fig. 5A, 5B). A significant reduction in serum viral titers in DGKα-deficient mice occurred as compared with WT controls (Fig. 5C). Despite the enhanced cellular activation, we did not detect evidence of an increased exhaustion, because there was no difference in the mean fluorescent intensity (MFI) of the inhibitory receptors PD-1 and LAG-3 between knockout and WT CD44^{+} gp33 tetramer^{+} CD8 T cells (Fig. 5D, 5E). These data suggest that a function of DGKα is to limit CD8 T cell activation, which is also a function of the ζ isoform (28). Because WT DGKζ is not inactivated in our system, this suggests an incomplete redundancy between these two isoforms in CD8 T cells. Finally, in the absence of DGKα, the increased frequency of activated, virus-specific CD8 T cells and reduced serum viral titers suggests that in viral infection, DGKα function normally dampens viral clearance. This may exist to limit self-detrimental inflammation in this state.

To determine the impact of an excessive CD8 T cell response to the mortality previously observed in early Clone 13 infection, we infected mice with LCMV Clone 13 that had previously received a chimeric bone marrow transplant with 7:3 admixture of marrow from a CD8$^{-/-}$ donor and either a WT or DGKα-deficient donor, respectively. After reconstitution, this model provides selective ablation of DGKα in the CD8 T cell compartment, while the remainder

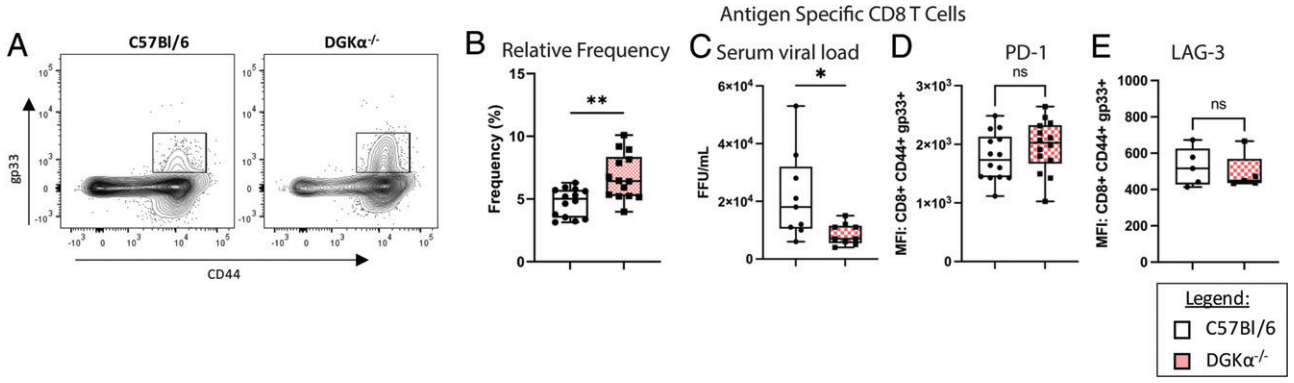

FIGURE 5. Relative and absolute frequencies of activated virus-specific (gp33 tetramer-bound) CD8 T cells on day 8 p.i. after LCMV Clone 13 infection. Representative flow plots and box and whisker plots for $CD44^+$, $gp33^+$ CD8 T cells (**A** and **B**), serum viral load (**C**), and MFI of PD-1 and LAG-3 checkpoint proteins (**D** and **E**). Box plots demonstrate interquartile range and median; whisker error bars are from minimum to maximum values. Relative frequency percentages in (B) are based on a ratio of the cell type listed to the following denominator listed in parentheses: Ag-specific CD8 T cells (CD8 splenocytes). Data presented in (A)–(D) are aggregated from three experiments with independent infections. Data presented in (E) represent a single infection. $*p < 0.05$, $**p < 0.01$.

of hemopoietic elements remain WT (Fig. 6A). In our system, after reconstitution of the chimera and before infection, peripheral blood CD8 T cells were observed at similar frequencies between the recipients of WT and DGK$\alpha^{-/-}$ CD8 T cells. Further, the CD8 T cell compartment demonstrated a chimera of donor and recipient cells, where at least 50% of the circulating CD8 T cells were derived from the donor (Supplemental Fig. 1). p.i. with LCMV Clone 13, mice with DGK$\alpha^{-/-}$ CD8 T cells suffered increased mortality as compared with controls (Fig. 6B). The median survival time after Clone 13 infection among mice with DGKα deficiency restricted to CD8 T cells was 23 d p.i. The findings in this chimeric system suggest that DGKα intrinsically limits CD8 T cell–mediated immunopathology, and its absence in CD8 T cells directly contributes to host death after LCMV Clone 13 infection.

Selective ablation of DGK$\alpha^{-/-}$ CD8 T cells rescues mice from immune-dysregulated mortality after LCMV Clone 13 infection

To further characterize the contribution of DGKα in mitigating CD8 T cell–mediated host mortality, we evaluated how selective, sustained depletion of CD8 T cells from mice globally deficient in DGKα would impact survival after Clone 13 infection (Fig. 7A). One day before LCMV Clone 13 infection and every 7 d thereafter, mice were treated with CD8-depleting Ab. Mice dosed with Ab were confirmed to have complete loss of CD8 T cells (Fig. 7B, 7C) 1 wk after initial Ab dosing. As expected, mice that were depleted of CD8 T cells were rescued from mortality after Clone 13 infection, whereas those who received PBS control all died (Fig. 7D). CD8-depleted mice also suffered significantly less weight loss than the CD8 replete group (Fig. 7E) and appeared to be more alert, active, and groomed than the CD8 replete group. These results suggest that DGK$\alpha^{-/-}$ CD8 T cells are necessary for the demise and mortality observed after LCMV Cl 13 infection in the global DGK$\alpha^{-/-}$ system.

DGKα limits signaling pathways associated with cell replication and effector function

To correlate the DGK$\alpha^{-/-}$ phenotype of CD8 T cells in early Clone 13 infection to an associated gene signature, we analyzed CD8 T cells with transgenic TCR specificity for an LCMV epitope, gp33, restricted to the murine MHC class I H-2D^b haplotype, known as P14 CD8 T cells (29). Eight days after Clone 13 infection and adoptive transfer of either WT P14 or DGK$\alpha^{-/-}$ P14 CD8 T cells into WT recipients, P14 T cells were enriched by flow cytometry–based sorting of splenocyte single-cell suspension by congenic marker for bulk RNA-seq.

Principal component analysis of WT P14 and DGK$\alpha^{-/-}$ P14 biologic replicates demonstrated separation of the two phenotypes along PC1 (Fig. 8A). GSEA was performed to identify differences in cellular signaling pathways observed among DGK$\alpha^{-/-}$ CD8 T cells compared with their WT counterparts. Notably, pathways enriched in

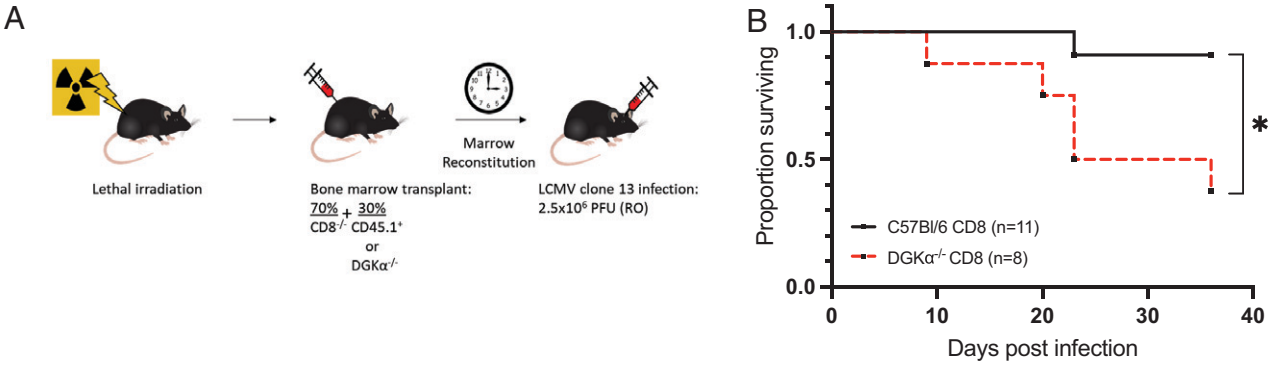

FIGURE 6. Characteristics of treatment cohorts p.i. with LCMV Clone 13. (**A**) Generation of bone marrow chimera. After irradiation and CD8 T cell depletion, mice were delivered a mixed bone marrow suspension by i.v. injection to generate hosts with DGKα deficiency restricted to CD8 T cells ($n = 8$) or control ($n = 11$). (**B**) Survival outcomes in bone marrow chimeric mice stratified by presence or absence of DGKα in CD8 T cells. Data presented were collected from two independent experiments and infections. $*p < 0.05$.

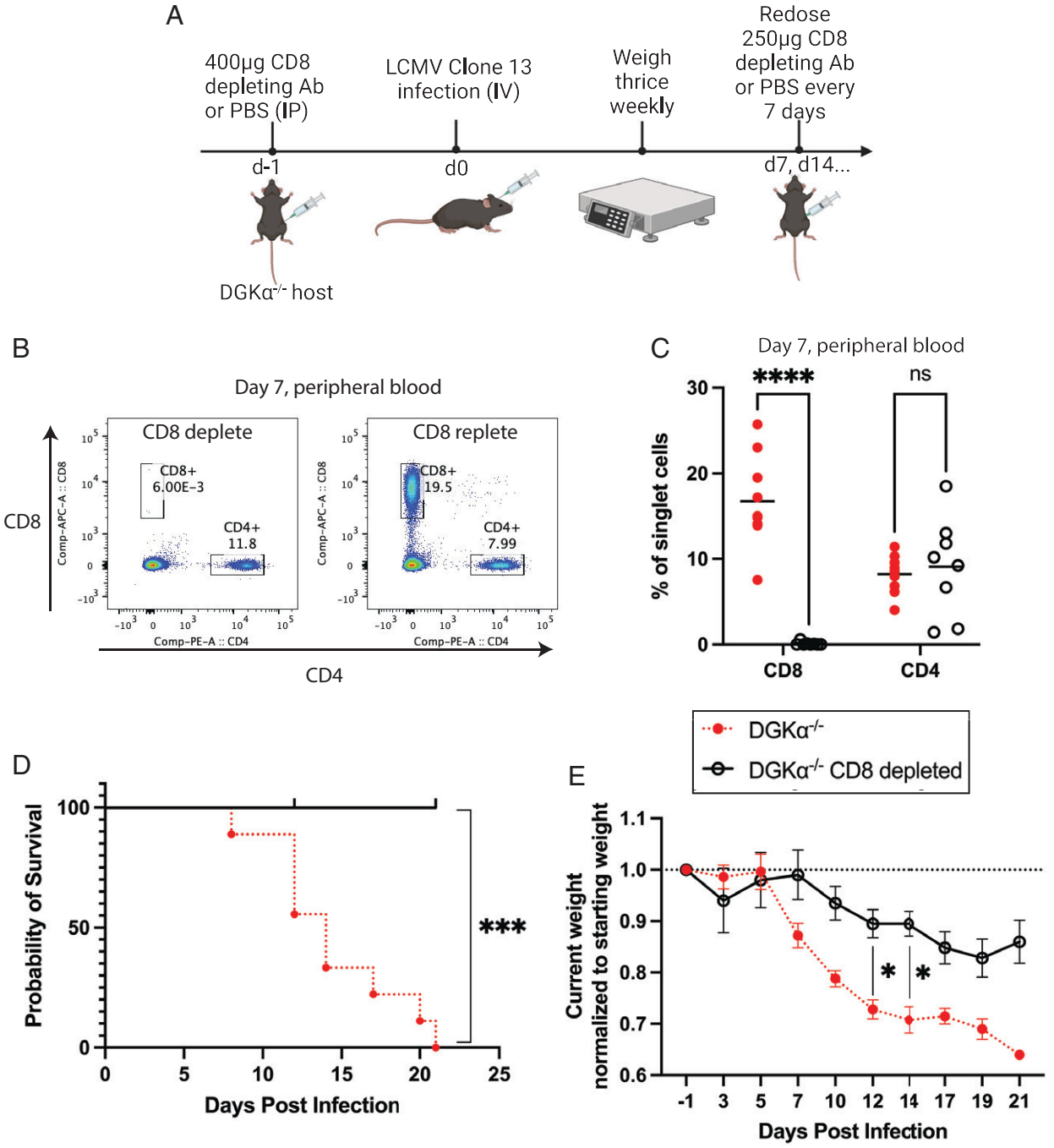

FIGURE 7. CD8 T cell depletion rescues mice globally deficient in DGKα from lethality after LCMV Clone 13 infection. The figure is representative of two experiments with independent infections and a total of $n = 7$ CD8-depleted and $n = 8$ CD8-replete (control) mice. (**A**) Experimental schema. (**B**) Representative flow plot of CD8 and CD4 T cell frequency in peripheral blood on day 7 after CD8 depletion. demonstrates absence of CD8 T cells in depleted host. (**C**) Comparison of frequency of CD8 and CD4 T cells recovered from peripheral blood on day 7 after CD8 T cell depletion. Relative frequency percentage is based on a ratio of the cell type listed to the total singlet splenocytes collected by flow cytometry as the denominator. (**D**) Kaplan–Meier survival curve stratified by CD8-depleted or -replete hosts. (**E**) Change in weight p.i. stratified by CD8-depleted or -replete hosts. Each data point is the mean weight; error bars represent SE of measurement. *$p < 0.05$, ***$p < 0.001$, ****$p < 0.0001$.

DGKα-deficient CD8 T cells included multiple unique cell-cycle signaling pathways, including gene sets related to cellular entry into prometaphase, assembly of mitotic spindles, and progression of cells through the S, G2, and M phases (Fig. 8B). A Venn diagram demonstrated the uniqueness of the enriched identified gene sets, with a 0–52% pairwise overlap between gene sets (Fig. 8C). In addition, genes associated with signaling through the mTOR complex 1 were also significantly enriched in the experimental cohort (net enrichment score = 1.53, $p_{adj} = 0.028$) (Supplemental Fig. 2A, 2B). Virus-specific DGKα$^{-/-}$ P14 CD8 T cells also demonstrated enhanced transcription of genes associated with glycolytic metabolism, effector function, and TCR signaling (Fig. 8D). These findings correlate with our phenotypic observation that DGKα functions to limit the expansion of virus-specific CD8 T cells (Fig. 5B) and suggests that this occurs through restriction of TCR signaling pathways and shunting cellular metabolism away from glycolytic processes.

To corroborate the observed transcriptional profiles with the phenotypic function of DGKα, we compared functional characteristics

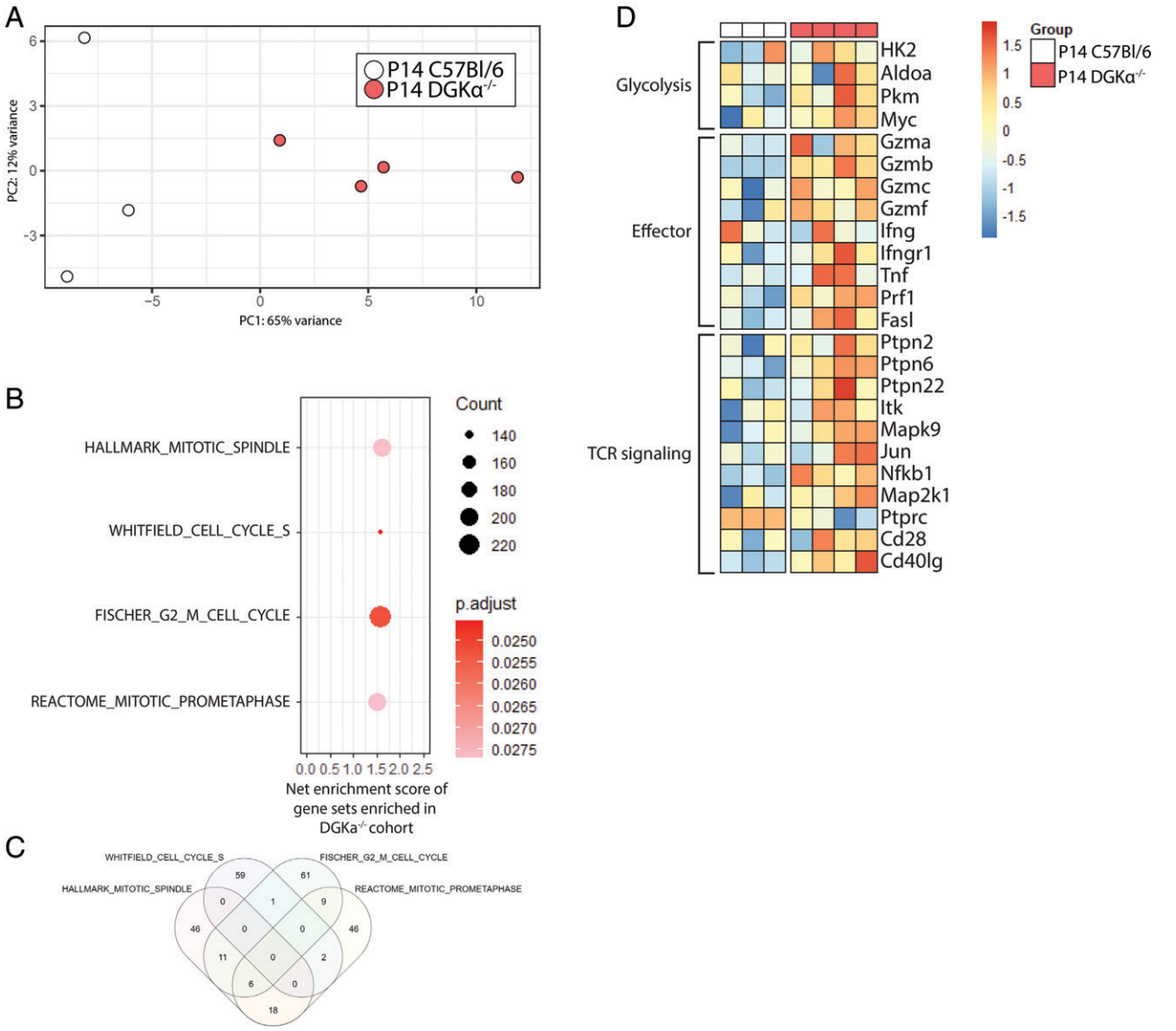

FIGURE 8. Bulk RNA-seq analysis of DGKα$^{-/-}$ and WT virus-specific CD8 T cells. On day 8 p.i. with LCMV Clone 13 and adoptive transfer of either congenic marked P14^{+} (n = 3) or P14^{+}, DGKα$^{-/-}$ (n = 4) CD8 T cells live, congenic marked CD8 splenocytes from each mouse were harvested and processed to generate a transcriptome library for bulk RNA-seq. (**A**) Principal component analysis of biologic replicates shows separation between experimental groups by first principal component (PC1). (**B**) Gene sets enriched among P14^{+}DGKα$^{-/-}$ CD8 T cells relative to WT P14 CD8 T cells. (**C**) Venn diagram demonstrating frequency of distinct genes among gene sets. (**D**) Heatmap of selected genes sorted by associated function.

of WT and DGKα-deficient P14 CD8 T cells in a competitive, in vivo setting. In an unstimulated state, WT P14 and DGKα P14 CD8 T cell subsets of naive (CD62L^{+}, CD44^{-}), effector memory (CD62L^{-}, CD44^{+}), and central memory (CD62L^{-}, CD44^{+}) were assessed and found to be in similar proportions to each other (Supplemental Fig. 3). After isolation of PBMCs from a P14 and P14-DGKα$^{-/-}$ donor, PBMC counts from each were normalized so that 2 × 10^{3} of each of P14 and P14DGKα$^{-/-}$ CD8 T cells were coadoptively transferred to recipient C57BL/6 hosts, and inoculation of LCMV Cl 13 was performed (Fig. 9A). Splenocytes collected on day 8 p.i. were analyzed by flow cytometry (Fig. 9B), revealing significantly elevated numbers of tetramer-positive, DGKα-deficient P14 T cells compared with P14 WT CD8 T cells (Fig. 9C). Further, a significant increase in granzyme B was observed on a per-cell basis among DGKα$^{-/-}$ CD8 T cells (Fig. 9D), and CD8 T cells lacking DGKα were the primary contributors of IFN-γ (Fig. 9E). DGKα-deficient P14 CD8 T cells also had enhanced per-cell production of IFN-γ as evidenced by MFI (Fig. 9F). These data confirm an enhanced effector phenotype of DGKα$^{-/-}$ P14 CD8 T cells as compared with P14 CD8 T cells after LCMV Clone 13 infection and support the observed changes in enhanced transcription of effector molecules in CD8 T cells in the absence of DGKα.

In summary, our data demonstrate that the deficiency of DGKα in a murine host leads to mortality after LCMV Clone 13 infection. Although the overwhelming immune response is likely multicellular in nature, CD8 T cells are a dominant effector of immune pathology in this system. Further DGKα$^{-/-}$ CD8 T cells are necessary for host mortality to occur after LCMV Clone 13 infection.

Discussion

We have demonstrated that DGKα is an essential regulator of CD8 T cell antiviral responses and plays an important role in balancing antiviral immunity with immunopathology in Clone 13 viral infection. After Clone 13 infection, we observed profound host mortality beginning in the second week of infection. This mortality occurred after Clone 13 infection in both systemic and CD8 T cell–restricted DGKα knockouts. The absence of DGKα regulation of TCR signaling enhances viral clearance and leads to increased splenic CD44^{+}, virus-specific CD8 T cells.

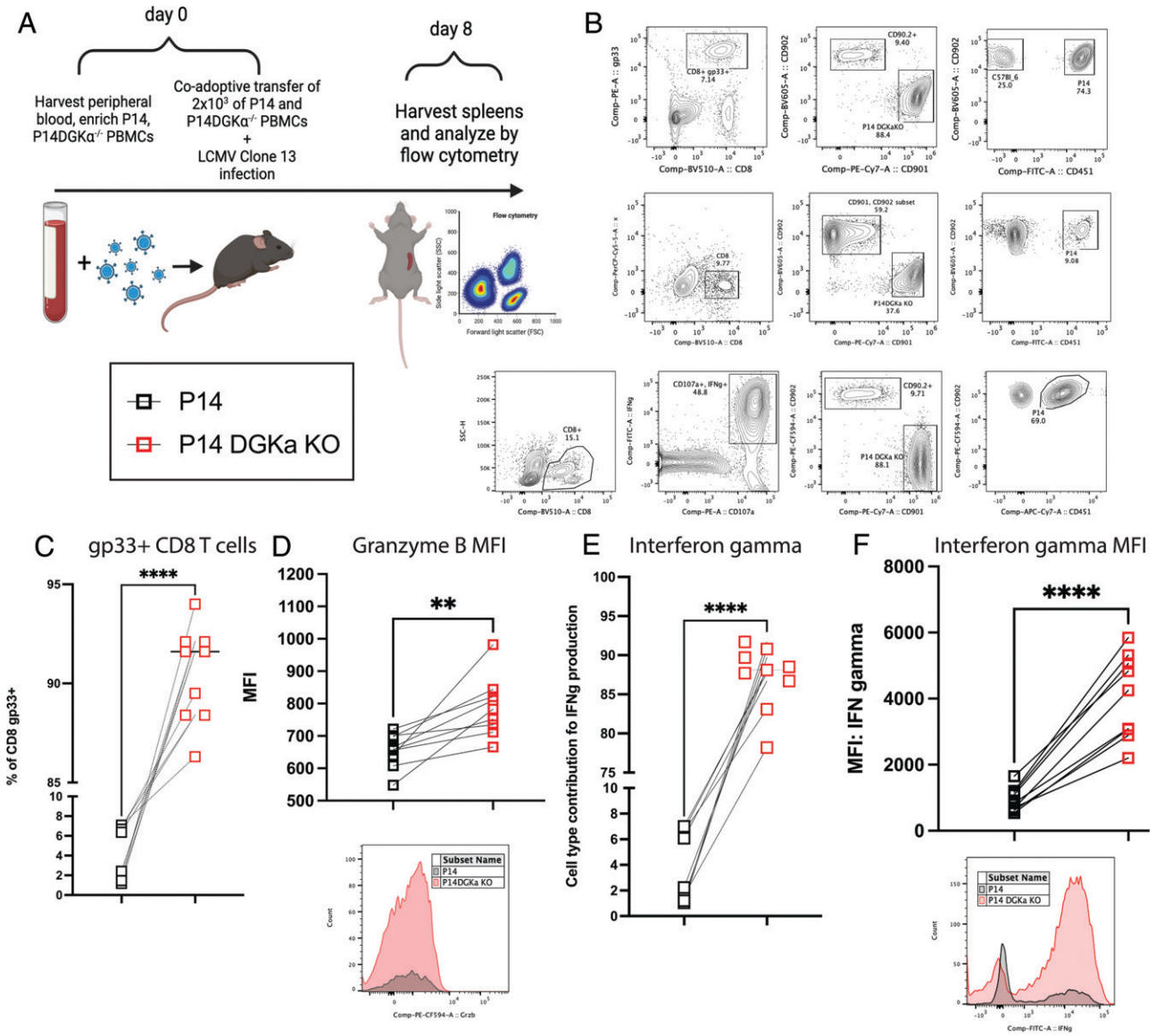

FIGURE 9. In vivo coadoptive transfer of congenic marked P14$^+$ and P14$^+$DGKα$^{-/-}$ enables direct comparison of virus-specific CD8 T cell expansion after LCMV Clone 13 infection. (**A**) Experimental schema. Splenocytes harvested and analyzed on day 8 p.i. and adoptive cell transfer. (**B**) Representative flow plots depicting gating strategy to identify P14$^+$ and P14$^+$DGKα$^{-/-}$ cell subsets among gp33 tetramer-positive (top row), mean fluorescent index (middle), and IFN-γ (IFNg)-producing CD8 T cells (bottom). (**C**) Paired analysis of composition of tetramer-positive CD8 T cells by origin. (**D**) Mean fluorescent index of granzyme B among activated CD8 T cells. (**E**) Paired analysis of the composition of IFN-γ-producing CD8 T cells by origin reveals P14$^+$DGKα$^{-/-}$ cells are principally responsible for IFN-γ production in this system. (**F**) P14$^+$DGKα$^{-/-}$ cells express higher per-cell IFN-γ than their P14 counterparts. Presented results are aggregated data of two separate experiments comprising a total of eight recipient mice. $^{**}p < 0.01$, $^{****}p < 0.0001$.

This profound activation did not appear to promote T cell exhaustion, because we did not observe increased expression of checkpoint proteins PD-1 and LAG-3. Finally, our data suggest that DGKα deficiency enhances mTOR cell signaling in virus-specific CD8 T cells and enhances transcription of genes associated with glycolytic metabolism, TCR signaling, and cytotoxic effector functions.

Previous studies have analyzed the role of DGKα in acute viral infection (14). Like in this study, we observed increases in virus-specific CD8 T cells among splenocytes and enhanced viral clearance in DGKα knockout. However, a key distinction between our study and studies evaluating the role of DGKα in acute viral infection is the profound mortality that occurred with Clone 13 infection. Oldstone et al. (30) recently demonstrated that Clone 13 infection also resulted in acute death in mouse models of immune dysregulation, including FVB, NZB, and PL/J strains. In these studies, mice had high numbers of antiviral CD8 T cells and increased levels of type I IFN (IFN-I), with death occurring as a result of enhanced pulmonary vascular permeability. Interestingly, blockade of IFN-I signaling CD8 prevented host death, as did CD8 T cell depletion. We similarly observed that in global DGKα knockout, depletion of CD8 T cells prevented host death after LCMV Clone 13 infection.

Although studies commonly focus on the role of T cells in immune pathology, they are likely not the exclusive cause of immunopathology and mortality. In the absence of DGKα, effector CD8 T cells are a dominant driver of immune pathology but are just one component of a dysregulated multicellular immune process that results in a lethal phenotype, because changes in the frequencies of myeloid, CD4 T cell, and B cell subtypes were also observed in our model.

A key limitation of our study is that we did not identify an organ-based cause of death in our model. Future studies incorporating tissue histology of vital organs, including lung, liver, and kidney, may identify an end organ dysfunction that may contribute to the cause of

death. In our model, although we did not analyze serum IFN-I levels, we observed nonsignificant elevations in serum TNF-α, which is a known proinflammatory cytokine and is associated with the pathogenesis of several autoimmune diseases, including rheumatoid arthritis, inflammatory bowel disease, and psoriatic arthritis (31). We also observed a nonsignificant increase in the circulating levels of IL-17 after LCMV Clone 13 infection in mice with DGKα deficiency as compared with WT. Others have shown that the combined absence of both α and ζ isoforms of DGK results in enhanced differentiation of Th17 CD4 T cells but does not occur if there is an isolated absence of either isoform (32). Because IL-17 is produced by a number of different immune cell subsets, including CD8 T cells (33), future studies of selective deficiency of DGKα in CD8 T cells can explore how IL-17–producing CD8 T cells may specifically contribute to this phenotype.

A potential mechanism of how DGKα-deficient CD8 T cells directly contribute to host mortality in Clone 13 infection may occur through resistance of DGKα$^{-/-}$ T cells to regulated TCR signaling. After TCR-mediated activation of CD8 T cells, protein tyrosine phosphatases (PTPs) SHP-1 and PTPN22 are recruited to the cell membrane to inactivate TCR-mediated phosphorylated Lck signaling. However, PTP dephosphorylation of Lck can be avoided, because strong TCR-mediated activation of CD8 T cells also triggers rapid and sustained ERK activity, which enables resistance of Lck protein to PTP-mediated dephosphorylation by altering the conformational structure of Lck (34). Although our transcriptomic data demonstrate upregulation of SHP-1 and PTPN22 PTPs in DGKα$^{-/-}$ CD8 T cells, our data also demonstrate transcriptional upregulation of ERK (encoded by *Mapk1*), suggesting that a potential mechanism of sustained TCR signaling occurs as a result of DAG-mediated rapid ERK production. In the absence of DAG inactivation from cleavage of DAG into phosphatidic acid by DGKα, sustained ERK production may inhibit PTPs from performing their usual function. Future studies characterizing temporal changes in intracellular DAG, ERK, and phosphorylated Lck levels after TCR activation of DGKα-deficient CD8 T cells would provide data to support this hypothesis.

In summary, DGKα is an indispensable regulator of TCR-mediated cellular activation in LCMV Clone 13 viral infection. We have demonstrated that DGKα functions to modulate cellular components of the adaptive immune response to early Clone 13 viral infection, most notably in CD8 T cells. When DGKα is absent, Clone 13 infection results in excessive cell cycling and proinflammatory processes, likely through upregulated mTOR complex 1, AP-1, and NF-κB–mediated pathways. Subsequently, infected mice succumb to a pathologic proinflammatory state and demise.

Acknowledgments

This research was completed in part with computational resources and technical support provided by the Research Computing Center at the Medical College of Wisconsin. Some aspects of figures were created with BioRender.com.

Disclosures

The authors have no financial conflicts of interest.

References

1. Wright, D. B., S. Tripathi, A. Sikarwar, K. T. Santosh, J. Perez-Zoghbi, O. O. Ojo, N. Irechukwu, J. P. T. Ward, and D. Schaafsma. 2013. Regulation of GPCR-mediated smooth muscle contraction: implications for asthma and pulmonary hypertension. *Pulm. Pharmacol. Ther.* 26: 121–131.
2. Joshi, R. P., and G. A. Koretzky. 2013. Diacylglycerol kinases: regulated controllers of T cell activation, function, and development. *Int. J. Mol. Sci.* 14: 6649–6673.
3. Wheeler, M. L., M. B. Dong, R. Brink, X. P. Zhong, and A. L. DeFranco. 2013. Diacylglycerol kinase ζ limits B cell antigen receptor-dependent activation of ERK signaling to inhibit early antibody responses. *Sci. Signal.* 6: ra91.
4. Chen, S. S., Z. Hu, and X. P. Zhong. 2016. Diacylglycerol kinases in T cell tolerance and effector function. *Front. Cell Dev. Biol.* 4: 130.
5. Chauveau, A., A. Le Floc'h, N. S. Bantilan, G. A. Koretzky, and M. Huse. 2014. Diacylglycerol kinase α establishes T cell polarity by shaping diacylglycerol accumulation at the immunological synapse. *Sci. Signal.* 7: ra82.
6. Mérida, I., E. Andrada, S. I. Gharbi, and A. Ávila-Flores. 2015. Redundant and specialized roles for diacylglycerol kinases α and ζ in the control of T cell functions. *Sci. Signal.* 8: re6.
7. Sakane, F., S. Mizuno, and S. Komenoi. 2016. Diacylglycerol kinases as emerging potential drug targets for a variety of diseases: an update. *Front. Cell Dev. Biol.* 4: 82.
8. Weber, H., S. Kittel-Schneider, A. Gessner, K. Domschke, M. Neuner, C. P. Jacob, H. N. Buttenschon, A. Boreatti-Hümmer, J. Volkert, S. Herterich, et al. 2011. Cross-disorder analysis of bipolar risk genes: further evidence of DGKH as a risk gene for bipolar disorder, but also unipolar depression and adult ADHD. *Neuropsychopharmacology* 36: 2076–2085.
9. Sim, J. A., J. Kim, and D. Yang. 2020. Beyond lipid signaling: pleiotropic effects of diacylglycerol kinases in cellular signaling. *Int. J. Mol. Sci.* 21: 6861.
10. Olenchock, B. A., R. Guo, J. H. Carpenter, M. Jordan, M. K. Topham, G. A. Koretzky, and X. P. Zhong. 2006. Disruption of diacylglycerol metabolism impairs the induction of T cell anergy. *Nat. Immunol.* 7: 1174–1181.
11. Arranz-Nicolás, J., J. Ogando, D. Soutar, R. Arcos-Pérez, D. Meraviglia-Crivelli, S. Mañes, I. Mérida, and A. Ávila-Flores. 2018. Diacylglycerol kinase α inactivation is an integral component of the costimulatory pathway that amplifies TCR signals. *Cancer Immunol. Immunother.* 67: 965–980.
12. Macián, F., C. García-Rodríguez, and A. Rao. 2000. Gene expression elicited by NFAT in the presence or absence of cooperative recruitment of Fos and Jun. *EMBO J.* 19: 4783–4795.
13. Atsaves, V., V. Leventaki, G. Z. Rassidakis, and F. X. Claret. 2019. AP-1 transcription factors as regulators of immune responses in cancer. *Cancers (Basel)* 11: 1037.
14. Shin, J., T. F. O'Brien, J. M. Grayson, and X.-P. Zhong. 2012. Differential regulation of primary and memory CD8 T cell immune responses by diacylglycerol kinases. *J. Immunol.* 188: 2111–2117.
15. Kahan, S. M., and A. J. Zajac. 2019. Immune exhaustion: past lessons and new insights from lymphocytic choriomeningitis virus. *Viruses* 11: 156.
16. Picelli, S., O. R. Faridani, A. K. Björklund, G. Winberg, S. Sagasser, and R. Sandberg. 2014. Full-length RNA-seq from single cells using Smart-seq2. *Nat. Protoc.* 9: 171–181.
17. Patro, R., G. Duggal, M. I. Love, R. A. Irizarry, and C. Kingsford. 2017. Salmon provides fast and bias-aware quantification of transcript expression. *Nat. Methods* 14: 417–419.
18. Love, M. I., W. Huber, and S. Anders. 2014. Moderated estimation of fold change and dispersion for RNA-seq data with DESeq2. *Genome Biol.* 15: 550.
19. Yu, G., L. G. Wang, Y. Han, and Q. Y. He. 2012. clusterProfiler: an R package for comparing biological themes among gene clusters. *OMICS* 16: 284–287.
20. Kanehisa, M., and S. Goto. 2000. KEGG: Kyoto encyclopedia of genes and genomes. *Nucleic Acids Res.* 28: 27–30.
21. Fabregat, A., S. Jupe, L. Matthews, K. Sidiropoulos, M. Gillespie, P. Garapati, R. Haw, B. Jassal, F. Korninger, B. May, et al. 2018. The Reactome Pathway Knowledgebase. *Nucleic Acids Res.* 46(D1): D649–D655.
22. Ashburner, M., C. A. Ball, J. A. Blake, D. Botstein, H. Butler, J. M. Cherry, A. P. Davis, K. Dolinski, S. S. Dwight, J. T. Eppig, et al.; The Gene Ontology Consortium. 2000. Gene Ontology: tool for the unification of biology. *Nat. Genet.* 25: 25–29.
23. Mills, K. H. G. 2008. Induction, function and regulation of IL-17-producing T cells. *Eur. J. Immunol.* 38: 2636–2649.
24. Norris, B. A., L. S. Uebelhoer, H. I. Nakaya, A. A. Price, A. Grakoui, and B. Pulendran. 2013. Chronic but not acute virus infection induces sustained expansion of myeloid suppressor cell numbers that inhibit viral-specific T cell immunity. *Immunity* 38: 309–321.
25. Maltby, S., N. G. Hansbro, H. L. Tay, J. Stewart, M. Plank, B. Donges, H. F. Rosenberg, and P. S. Foster. 2014. Production and differentiation of myeloid cells driven by proinflammatory cytokines in response to acute pneumovirus infection in mice. *J. Immunol.* 193: 4072–4082.
26. Wang, C., N. Zhang, L. Qi, J. Yuan, K. Wang, K. Wang, S. Ma, H. Wang, W. Lou, P. Hu, et al. 2017. Myeloid-derived suppressor cells inhibit T follicular helper cell immune response in Japanese encephalitis virus infection. *J. Immunol.* 199: 3094–3105.
27. Sanjuán, M. A., D. R. Jones, M. Izquierdo, and I. Mérida. 2001. Role of diacylglycerol kinase α in the attenuation of receptor signaling. *J. Cell Biol.* 153: 207–220.
28. Zhong, X. P., E. A. Hainey, B. A. Olenchock, M. S. Jordan, J. S. Maltzman, K. E. Nichols, H. Shen, and G. A. Koretzky. 2003. Enhanced T cell responses due to diacylglycerol kinase ζ deficiency. *Nat. Immunol.* 4: 882–890.
29. Pircher, H., D. Moskophidis, U. Rohrer, K. Bürki, H. Hengartner, and R. M. Zinkernagel. 1990. Viral escape by selection of cytotoxic T cell-resistant virus variants in vivo. *Nature* 346: 629–633.
30. Oldstone, M. B. A., B. C. Ware, L. E. Horton, M. J. Welch, R. Aiolfi, A. Zarpellon, Z. M. Ruggeri, and B. M. Sullivan. 2018. Lymphocytic choriomeningitis virus Clone 13 infection causes either persistence or acute death dependent on IFN-1, cytotoxic T lymphocytes (CTLs), and host genetics. *Proc. Natl. Acad. Sci. USA* 115: E7814–E7823.
31. Jang, D. I., A. H. Lee, H. Y. Shin, H. R. Song, J. H. Park, T. B. Kang, S. R. Lee, and S. H. Yang. 2021. The role of tumor necrosis factor alpha (Tnf-α) in autoimmune disease and current tnf-α inhibitors in therapeutics. *Int. J. Mol. Sci.* 22: 2719.
32. Yang, J., H. X. Wang, J. Xie, L. Li, J. Wang, E. C. K. Wan, and X. P. Zhong. 2020. DGK α and ζ activities control T_H1 and T_H17 cell differentiation. *Front. Immunol.* 10: 3048.
33. Srenathan, U., K. Steel, and L. S. Taams. 2016. IL-17+ CD8+ T cells: differentiation, phenotype and role in inflammatory disease. *Immunol. Lett.* 178: 20–26.
34. Fowler, C. C., L. I. Pao, J. N. Blattman, and P. D. Greenberg. 2010. SHP-1 in T cells limits the production of CD8 effector cells without impacting the formation of long-lived central memory cells. *J. Immunol.* 185: 3256–3267.